SIMULATION OF IONOSPHERIC EFFECTS FROM ACOUSTIC WAVES PRODUCED BY EXPLOSIVE EVENTS AT GROUND SURFACE

Sergey Fridman and L. J. Nickisch

NorthWest Research Associates, 301 Webster St., Monterey, CA 93940, sergey@nwra.com

A growing number of observations appear to suggest that earthquakes and powerful explosions at ground surface may cause noticeable perturbations in the ionosphere. The earliest (in arrival time) explosion-related ionospheric effects are attributed to the infrasound (acoustic) waves. It is believed that internal gravity waves arrive with a considerable delay after the acoustic pulse. According to some reports the ionospheric effects from acoustic pulses are discernable in time series of GPS TEC data collected by ground-based TEC receivers. While observational research on correlation of ionospheric effects with explosive events are abundant, there is still scientific need to confirm existence of such effects in physics-based simulations. In this paper we present simulation of propagation of acoustic pulses generated by explosions or earthquakes. The simulation employs realistic model of the background atmosphere, ionosphere, and wave dissipation. The acoustic pulse propagation model is based on ray approximation, and employs appropriate dispersion relationship for atmospheric waves. We simulate the GPS TEC response to an earthquake event, and observe that characteristic features of simulated TEC time series are similar to those reported in observations.

1. INTRODUCTION

A number of observations appear to suggest that earthquakes and powerful explosions at ground surface (henceforth referred to as explosive events) may cause noticeable perturbations in the ionosphere (Afraimovich and Astafieva 2002; Afraimovich et al. 2013). In this paper we are attempting to perform physics-based simulation of ionospheric electron density perturbations driven by the impact of explosive events at the ground level. The earliest (in arrival time) and most distinct explosive event-related ionospheric effects are attributed to infrasound (acoustic) waves, so we will concentrate on modelling effects associated with this branch of atmospheric oscillations. Most of the observations of explosive event-related ionospheric effects come from analyzing of TEC time series from GPS receivers, so we will model manifestation of the acoustic pulses in TEC data.

2. SIMULATION OF ATMOSPHERIC WAVES EXCITED BY EXPLOSIVE EVENT IN REALISTIC ATMOSPHERE

The dispersion relation of acoustic-gravity waves exhibits two distinct branches – the acoustic branch and the gravity wave branch (Yeh and Liu 1972). The waves of the gravity branch are characterized by low (sub-sonic) phase velocities, so that oscillations within this branch can be excited and sustained by small-scale and medium-scale meteorological phenomena, such as convection cells. The acoustic branch is characterized by fast (super-sonic) phase velocities, so that this branch cannot be efficiently excited by any meteorological motion. Explosive events are known to excite both branches.

In order to estimate the acoustic field within a realistic model of the atmosphere we employ the geometrical optics approximation. In the implementation of the method presented here, every component of the field *f* is represented as a superposition of partial waves with different frequencies:

$$f(\mathbf{r},t) = \mathrm{Re}\int_0^\infty F(\mathbf{r},\omega)e^{-i\omega[t-\tau_p(\mathbf{r},\omega)]}d\omega \qquad (1)$$

where $F(\mathbf{r},\omega)$ is the smoothly-varying wave amplitude function which accounts for focusing, attenuation, and the wave radiation arrangement, $\tau_P(\mathbf{r},\omega)$ is the field of phase delay which is related to the eikonal $\varphi(\mathbf{r},\omega)$ as $\varphi(\mathbf{r},\omega)=\omega\tau_P(\mathbf{r},\omega)$.

Functions $\tau_P(\mathbf{r},\omega)$ and $F(\mathbf{r},\omega)$ are estimated with the help of acoustic ray tracing as describe below.

Ray tracing equations for acoustic waves in the atmosphere. We are employing Hamiltonian formulation of ray-tracing equations for stationary atmosphere. In Cartesian coordinates the equations may be formulated as follows.

$$\begin{aligned}\frac{d}{d\tau}\mathbf{R} &= -\frac{\partial \mathrm{H}}{\partial \mathbf{k}}\Big/\frac{\partial \mathrm{H}}{\partial \omega}\\ \frac{d}{d\tau}\mathbf{k} &= \frac{\partial \mathrm{H}}{\partial \mathbf{R}}\Big/\frac{\partial \mathrm{H}}{\partial \omega}\end{aligned} \qquad \textbf{(2)}$$

In these equations $\mathbf{R}(\tau)$ is the ray path trajectory, τ is the group delay along the ray path, $\mathbf{k}(\tau)$ is the wave vector along the path, and $\mathrm{H}(\mathbf{k},\omega)$ is the Hamiltonian function. We employ the following form of the Hamiltonian

$$\mathrm{H}=\frac{c_s^2(k^2+k_a^2)}{4}\left[1+\sqrt{1-\frac{4\omega_B^2(k^2-k_z^2)}{c_s^2(k^2+k_a^2)^2}}\right]-\frac{\omega^2}{2} \qquad \textbf{(3)}$$

where c_s is the speed of sound, $\mathbf{k}$ is the wave vector, $k_z=\mathbf{k}\cdot\hat{\mathbf{z}}$ is the vertical component of the wave vector, $k=\sqrt{\mathbf{k}\cdot\mathbf{k}}$, γ is the specific heat ratio, $\omega_B=\sqrt{\gamma-1}g/c_s$ is the buoyancy frequency, $k_a=\gamma g/2c_s^2=1/2h$, g is the acceleration of gravity, $h=c_s^2/\gamma g$ is the atmospheric scale height.

Thus, the equation $\mathrm{H}(\mathbf{k},\omega)=0$ is equivalent to the dispersion relation for acoustic waves

$$\begin{aligned}\omega^2 &= W_A^2(\mathbf{k})\\ W_A(\mathbf{k}) &= \sqrt{\frac{c_s^2(k^2+k_a^2)}{2}\left[1+\sqrt{1-\frac{4\omega_B^2(k^2-k_z^2)}{c_s^2(k^2+k_a^2)^2}}\right]}\end{aligned} \qquad \textbf{(4)}$$

In order to be able to calculate the phase delay τ_P we augment equations (2) with the phase equation

$$\frac{d}{d\tau}\tau_P=\frac{1}{\omega}\mathbf{k}\cdot\mathbf{v}_G \qquad \textbf{(5)}$$

where

$$\mathbf{v}_G=-\frac{\partial \mathrm{H}}{\partial \mathbf{k}}\Big/\frac{\partial \mathrm{H}}{\partial \omega} \qquad \textbf{(6)}$$

is the group velocity.

Focusing and attenuation of atmospheric waves. We are treating attenuation effects as small perturbation. Then the phase delay is evaluated disregarding the dissipative effects. The attenuation is factored into $F(\mathbf{r},\omega)$ via the attenuation index μ:

$$F(\mathbf{r},\omega) = F_0(\mathbf{r},\omega)e^{-\mu} \tag{7}$$

Here $F_0(\mathbf{r},\omega)$ is the amplitude factor at dissipation-free propagation. This factor may be derived using the concept of power flow preservation along ray tubes (Nickisch 1988):

$$F_0(\mathbf{R},\omega) = A(\theta,\phi,\omega)\sqrt{\left|\frac{1}{v_G^2}\mathbf{v}_G \cdot \left[\frac{\partial \mathbf{v}_G}{\partial\theta}\times\frac{\partial \mathbf{v}_G}{\partial\phi}\right]_{\tau=0}\right| \Big/ \left|\mathbf{v}_G \cdot \left[\frac{\partial \mathbf{R}}{\partial\theta}\times\frac{\partial \mathbf{R}}{\partial\phi}\right]_{\tau=\tau'}\right|} \tag{8}$$

Here angles θ and ϕ specify exit direction for the ray that reaches point $\mathbf{R}$, τ' is the group delay of the ray when it crosses point $\mathbf{R}$, $A(\theta,\phi,\omega)$ identify the frequency-dependent radiation pattern of the source, and the square root term is the focusing factor for waves radiated by a point source.

The attenuation index is equal to the wave decrement $\chi(\mathbf{R},\mathbf{k},\omega)$ accumulated along the ray trajectory. In other words the attenuation may be derived by augmenting the system of ray-tracing equations (2), (5) with the following equation

$$\frac{d\mu}{d\tau} = \chi(\mathbf{R},\mathbf{k},\omega) \tag{9}$$

The decrement can be derived from the dispersion relationship that takes into account dissipation processes. We followed the analysis of dissipative dispersion relationship of atmospheric waves by (Godin 2014) to formulate $\chi(\mathbf{R},\mathbf{k},\omega)$. The resulting dissipation characteristics are consistent with those commonly used in simulations of atmospheric waves (Vadas 2007; Godin 2014).

The atmospheric temperature profile is adopted as the analytical model suggested by (Vadas and Fritts 2006)

$$T(z) = T_{\max} + (T_0 - T_{\max})\left[\frac{1}{2}\left(1-\tanh\left(\frac{z-z_\Delta}{\Delta}\right)\right)\right]^{0.2} \tag{10}$$

with $T_0 = 246\ K$, $T_{\max} = 1000\ K$, Δ=16 km, z_Δ=112 km.

Radiation pattern from a localized impact. Consider evolution of a localized initial perturbation of atmospheric density in sufficiently close vicinity of the impact. "Sufficiently close" means that the atmosphere may be treated as isothermal and dissipation-free. The initial perturbation has the form

$$f(\mathbf{r},0) = \delta(\mathbf{r}) \tag{11}$$

Here $\delta(\mathbf{r})$ is the three-dimensional Dirac's function. The perturbation in sufficiently close vicinity at time *t* may be represented as a superposition of plane waves

$$f(\mathbf{r},t)=\frac{1}{(2\pi)^3}\iiint e^{i[\mathbf{k}\cdot\mathbf{r}-\overline{W}_A(\mathbf{k})t]}d^3\mathbf{k} \qquad \textbf{(12)}$$

where $\overline{W}_A(\mathbf{k})=W_A(\mathbf{k})\big|_{\mathbf{r}=0}$. We are assuming for simplicity that the perturbation excites acoustic mode only. The asymptotic behavior of this function (formally at $|\mathbf{r}|\to\infty$) may be evaluated with the help of the stationary phase method, yielding

$$f(\mathbf{r},t)=\int A(\hat{\mathbf{r}},\omega)e^{i\left[r\overline{K}_A(\omega,\hat{\mathbf{r}})-\omega t\right]}\frac{1}{r}d\omega \qquad \textbf{(13)}$$

Where $\overline{K}_A(\omega,\hat{\mathbf{k}})$ is defined by the equation $\overline{W}_A[\hat{\mathbf{k}}\overline{K}(\omega,\hat{\mathbf{k}})]=\omega$, $\hat{\mathbf{r}}=\mathbf{r}/|\mathbf{r}|$, $\hat{\mathbf{k}}=\mathbf{k}/|\mathbf{k}|$, and

$$A(\hat{\mathbf{k}},\omega)=\frac{1}{(2\pi)^2 i}\overline{K}_A(\omega,\hat{\mathbf{k}})\left|\hat{\mathbf{k}}\cdot\mathbf{v}_G(\omega,\hat{\mathbf{k}})\right|^{-1}\Big|_{\mathbf{r}=0} \qquad \textbf{(14)}$$

Comparing this expression with (1) and (8), taking into account that the focusing factor in (8) for the case of isothermal atmosphere amounts to 1/*r*, we conclude that indeed $A(\hat{\mathbf{k}},\omega)$ represents the radiation pattern.

Construction of the wave solution in the geometrical optics approximation. In the simulations presented here we neglect effects of the wind on sound propagation and we assume that the atmosphere is horizontally uniform. We adopt sufficiently wide and dense set of wave frequencies. For every wave frequency ω we perform solution of ray-tracing equations (2), (5), (9) at various elevation angles θ of the initial wave vector. As a result we obtain a set of functions $\mathbf{R}(\tau.\theta)$, $\mathbf{k}(\tau.\theta)$, $\tau_p(\tau.\theta)$, and $\mu(\tau.\theta)$. Then, the function $\mathbf{R}(\tau.\theta)=\left[X(\tau.\theta),0,Z(\tau.\theta)\right]$ is inverted, so that the functions $\tau(x,z),\theta(x,z)$ such that $\mathbf{R}\left[\tau(\mathbf{r}),\theta(\mathbf{r})\right]=\mathbf{r}$ are produced. These functions allow to derive $\tau_p(\mathbf{r})=\tau_p(\tau(\mathbf{r}),\theta(\mathbf{r}))$, and $\mu(\mathbf{r})=\mu(\tau(\mathbf{r}),\theta(\mathbf{r}))$ which, in turn, allow to establish $\varphi(\mathbf{r},\omega)$ and $\mu(\mathbf{r},\omega)$. The focusing part of the expression (8) is evaluated by exploiting the axial symmetry of the solution and approximating derivatives over θ with appropriate first-difference estimates.

Thus, the wave solution (1) is assembled with the help of (7), (8), and (14).

Air motion in acoustic waves. The numerical solution process outlined above ends up producing solution (1) for perturbation of atmospheric mass density. In order to simulate ionospheric effects of atmospheric waves we need to derive the field of air velocity associated with the waves. For this purpose we employ the polarization relations for AGWs, namely expression (8.4.7) of *Yeh and Liu* [1972], to express all desired components of the wave in terms of functions $\varphi(\mathbf{r},\omega)$ and $F(\mathbf{r},\omega)$.

$$\begin{bmatrix}\dfrac{\rho'(\mathbf{r},t)}{\rho_0(z)}\\ v_x(\mathbf{r},t)\\ v_z(\mathbf{r},t)\end{bmatrix}=\sqrt{\frac{\rho_0(0)}{\rho_0(z)}}\,\mathrm{Re}\int_0^\infty\begin{bmatrix}\omega^2(-k_z-ik_a)+i(\gamma-1)gk_x^2\\ \omega k_x(-k_z c_s^2+ig(\gamma/2-1))\\ -\omega(\omega^2-k_x^2c_s^2)\end{bmatrix}\frac{F(\mathbf{r},\omega)e^{i[\varphi(\mathbf{r},\omega)-\omega t]}d\omega}{\omega^2(-k_z-ik_a)+i(\gamma-1)gk_x^2} \qquad \textbf{(15)}$$

This expression provides the relative perturbation of mass density $\frac{\rho'(\mathbf{r},t)}{\rho_0(z)}$ along with the vertical $v_z(\mathbf{r},t)$ and horizontal $v_x(\mathbf{r},t)$ components of the air velocity.

Ionospheric manifestations of atmospheric infrasound generated by explosive events. When infrasonic waves travel through the ionosphere, the electrons and ions are dragged by the motion of neutral air. The direction of motion of charged particles is confined to the direction along the geomagnetic field. It means that the neutral air moving with a velocity vector v, induces plasma motion with velocity

$$\mathbf{v}_p = \hat{\mathbf{b}}(\hat{\mathbf{b}} \cdot \mathbf{v}) \tag{16}$$

[*Yeh and Liu*, 1972]. Here $\hat{\mathbf{b}}$ is the unit vector along the magnetic field direction. This motion redistributes ionospheric plasma in accordance with the continuity equation

$$\frac{\partial}{\partial t} n_e + \nabla \cdot \mathbf{v}_p n_e = 0 \tag{17}$$

In order to estimate the field of perturbation of plasma density δn_e, we will employ the linearized version of the continuity equation, then $n_e = N_e + \delta n_e$,

$$\delta n_e(\mathbf{r},t) = -N_e \hat{\mathbf{b}} \cdot \int_{-\infty}^{t} dt' \nabla(\hat{\mathbf{b}} \cdot \mathbf{v}) - \frac{\partial N_e}{\partial z} \hat{b}_z \hat{\mathbf{b}} \cdot \int_{-\infty}^{t} dt' \mathbf{v} \tag{18}$$

Where the unperturbed electron density distribution $N_e(z)$ is assumed to be stationary and horizontally-stratified.

3. RESULTS AND CONCLUSIONS

In order to demonstrate ionospheric perturbations driven by infrasound waves we utilized the atmospheric motion solution as described above. In the results presented here the solution is scaled up to represent the displacement of 3x10^6 kg of air. The adopted background electron density profile represents daytime conditions in accordance with IRI2007.

Electron density perturbations derived for the vertical plane of the magnetic meridian are shown in Figure 1. In this simulation we adopted the magnetic dip angle of *I*=30 degrees. We observe that the perturbation of electron density does not preserve axial symmetry of the underlying atmospheric motion. Ionospheric perturbations to the South of the impact point are noticeably stronger than the perturbations on the Northern side. It happens because air motion tends to be better aligned with the geomagnetic field direction at locations southward of the impact.

Another interesting observation is that after about 10 minutes from the impact, the ionospheric perturbations in E- and F-regions of the ionosphere become isolated from each other by an altitude gap where plasma is not perturbed. This gap widens with time. The gap is a manifestation of the acoustic shadow region that separates obliquely propagating acoustic waves that reflect from the temperature increase at about 100 km altitude, from the waves radiated in near-vertical direction which propagate

without experiencing reflection. The perturbation in E-region propagates as a localized disturbance with horizontal size of the order of one kilometer.

Figure 3 and Figure 4 show results of simulating time series of slant TEC for various fixed lines of sight. The lines of sight are identified in Figure 2. All selected lines of sight lie within the plane of magnetic meridian that contain the point of impact.

Figure 3 shows TEC for a receiver located 500 km south of the point of impact. This line of sight is tilted at 45 degrees elevation angle. These variations of slant TEC look strikingly similar to observations reported by (Afraimovich and Astafieva 2002) in connection with earthquake events.

Figure 4 shows simulated TEC observations for a receiver positioned 400 km south of the point of impact. We note that now, at the same elevation of the line of sight the temporal scale of TEC variations becomes faster, while the amplitude of variations increases. We also note a burst of fast TEC oscillations that starts at t=1000 seconds and lasts for 30 seconds. This burst may be traced to the event of crossing the line of sight by the localized electron density perturbation in E-region as it is illustrated in Figure 2. Corresponding vertical line of sight (Figure 4) shows considerably weaker TEC perturbations than the oblique path. It happens because the oblique paths that we considered happen to become nearly parallel to the wave front of the acoustic wave at certain time. It is around this time that the most prominent TEC signals are observed. The vertical line of sight, on the other hand, is never parallel to the wave front, so that enhancements of electron density along the line of sight are virtually compensated by depressions, resulting in weak overall TEC signal.

REFERENCES

Afraimovich, E. L., and E. I. Astafieva. 2002. “Isolated Ionospheric Disturbances as Deduced from Global GPS Network.” *arXiv Preprint Physics/0212021*. https://arxiv.org/abs/physics/0212021.

Afraimovich, Edward L., Elvira I. Astafyeva, Vladislav V. Demyanov, Ilya K. Edemskiy, Nadezhda S. Gavrilyuk, Artem B. Ishin, Eugene A. Kosogorov, et al. 2013. “A Review of GPS/GLONASS Studies of the Ionospheric Response to Natural and Anthropogenic Processes and Phenomena.” *Journal of Space Weather and Space Climate* 3: A27. doi:10.1051/swsc/2013049.

Godin, Oleg A. 2014. “Dissipation of Acoustic-Gravity Waves: An Asymptotic Approach.” *The Journal of the Acoustical Society of America* 136 (6): EL411-EL417. doi:10.1121/1.4902426.

Nickisch, L. J. 1988. “Focusing in the Stationary Phase Approximation.” *Radio Science* 23 (2): 171–82. doi:10.1029/RS023i002p00171.

Vadas, Sharon L. 2007. “Horizontal and Vertical Propagation and Dissipation of Gravity Waves in the Thermosphere from Lower Atmospheric and Thermospheric Sources: GRAVITY WAVES IN THE THEMOSPHERE.” *Journal of Geophysical Research: Space Physics* 112 (A6): n/a-n/a. doi:10.1029/2006JA011845.

Vadas, Sharon L., and David C. Fritts. 2006. “Influence of Solar Variability on Gravity Wave Structure and Dissipation in the Thermosphere from Tropospheric Convection.” *Journal of Geophysical Research* 111 (A10). doi:10.1029/2005JA011510.

Yeh, K. C., and C. H. Liu. 1972. *Theory of Ionospheric Waves*. International Geophysics Series, v. 17. New York: Academic Press.

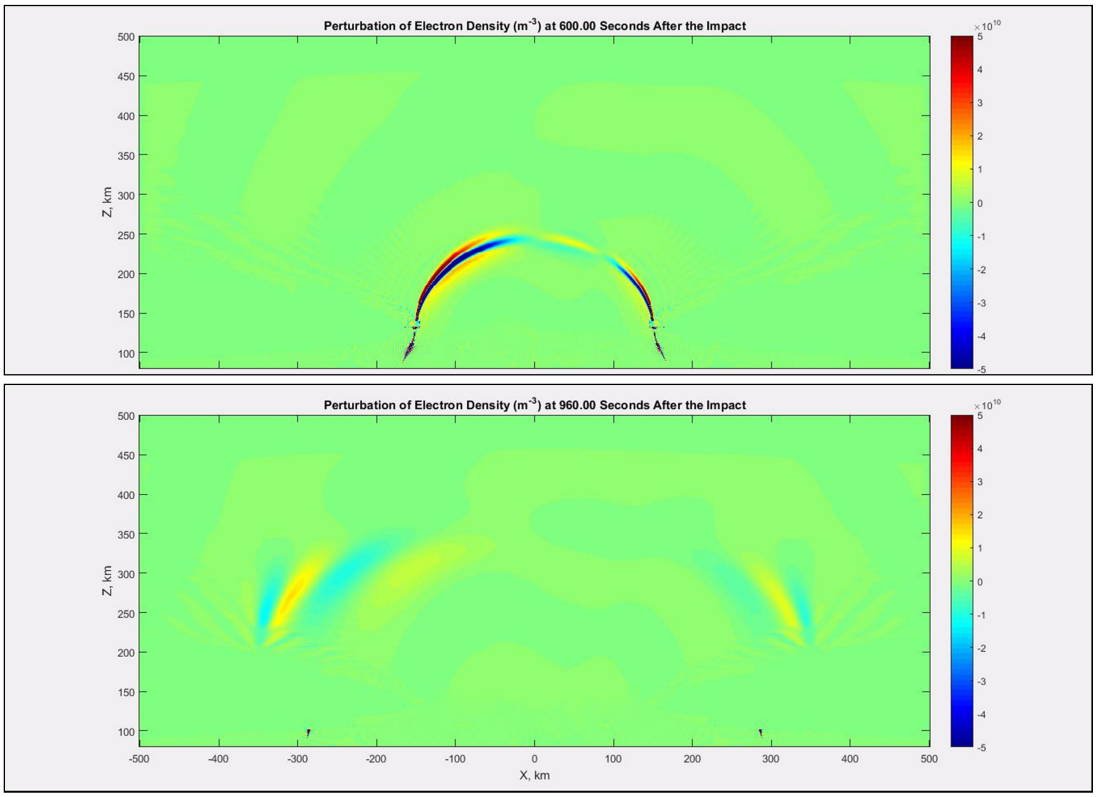

Figure 1. **Vertical cross-sections of electron density perturbations along the plane of magnetic meridian for the atmospheric perturbation described in text. The horizontal axis shows ground-distance from the impact location**

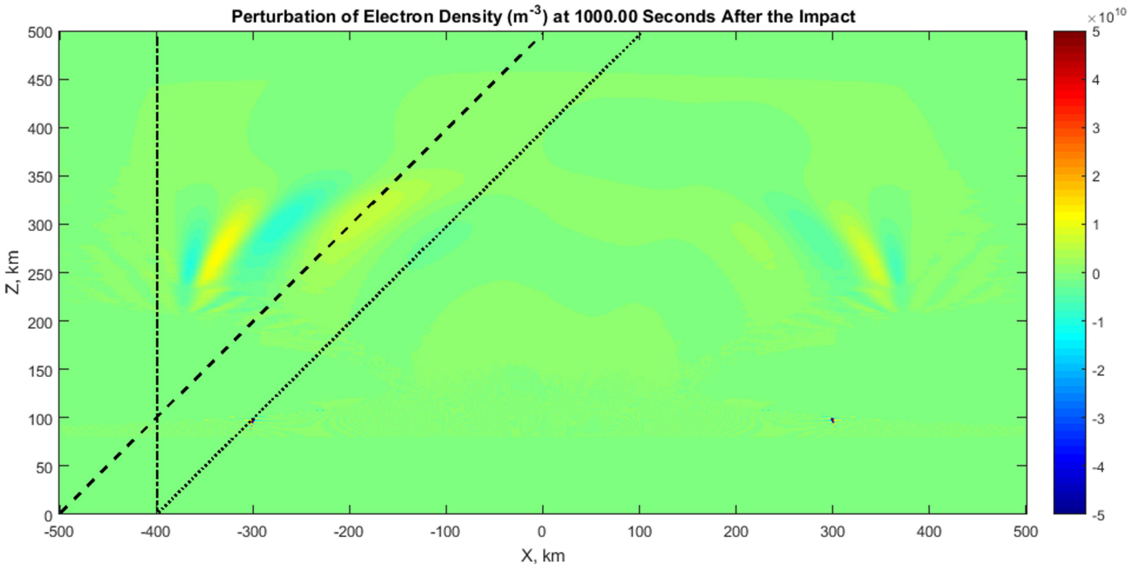

Figure 2. **Lines of sight for slant TEC simulation (dashed lines)**

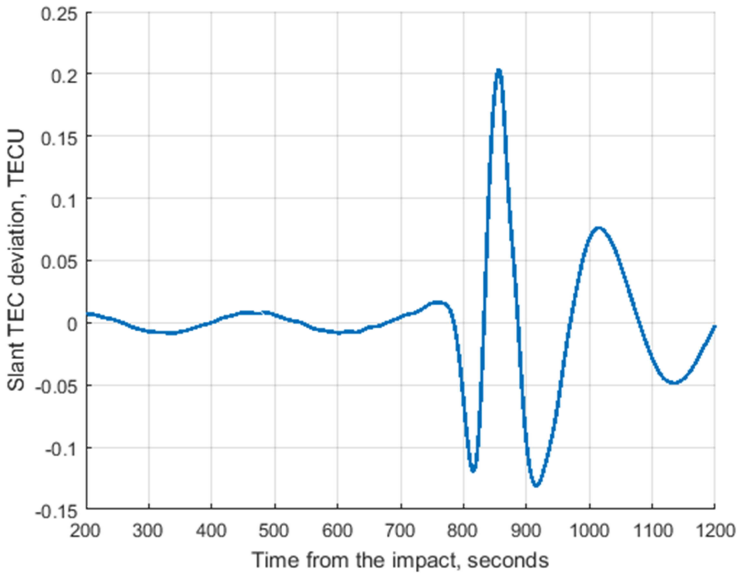

Figure 3. **Time series of deviations of slant TEC from background values for the line of sight shown by dashed line in Figure 2**

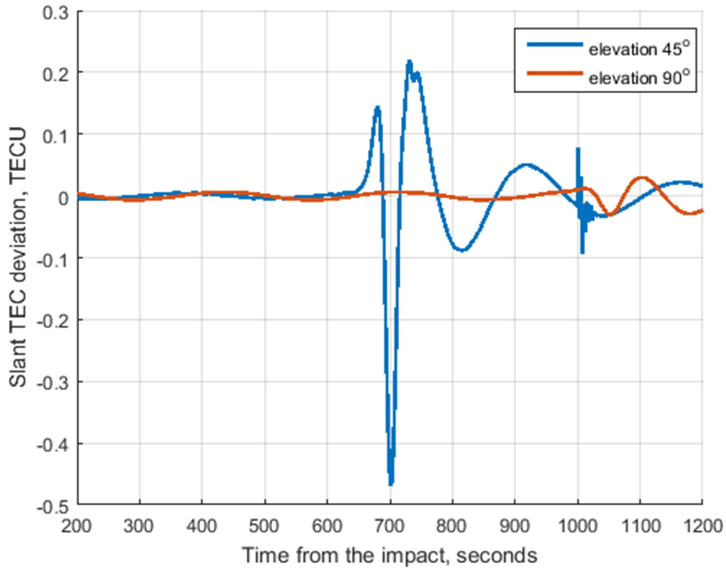

Figure 4. **Time series of deviations of slant TEC from background values for lines of sight shown by dotted (elevation 45 degrees) and dash-dotted (elevation 90 degrees) lines in Figure 2**